

Optimal Analysis for Shakedown of Functionally Graded (FG) Bree Plate with Genetic Algorithm

H. Zheng^{1,2}, X. Peng^{1,2,3,4} and N. Hu^{1,3,5}

Abstract: The Shakedown of a functionally graded (FG) Bree plate subjected to coupled constant mechanical loading and cyclically varying temperature is analyzed with more accurate approaches and optimized with the genetic algorithm method. The shakedown theorem takes into account material hardening. The variation of the material properties in the thickness of a FG Bree plate is characterized with a piecewise exponential distribution, which can replicate the actual distribution with sufficient accuracy. In order to obtain the best distribution of the mechanical properties in the FG plate, the distribution of the reinforcement particle volume fraction is optimized with the genetic algorithm (GA). Two numerical examples are presented, which demonstrate the validity of the developed method in the analysis of the shakedown of the FG Bree plate.

Keywords: Functionally graded Bree plate, Coupled thermal-mechanical loading, Shakedown, Optimization, Genetic algorithm.

1 Introduction

The rapid development of aircraft and space technologies requires materials to work in more and more severe environments, such as high and varying temperature with large temperature gradients. With the distributions of the thermal and mechanical properties properly designed according to the requirements in practical applications, functionally graded materials (FGMs) play an irreplaceable role in improving the performance of the composite materials. The gradient distribution of the thermal

¹ Department of Engineering Mechanics, Chongqing University, Chongqing, 400044, China.

² Chongqing Key Laboratory of Heterogeneous Material Mechanics, Chongqing University, Chongqing, 400044, China.

³ College of Aerospace Engineering, Chongqing University, Chongqing, 400044, China.

⁴ Corresponding author, Email: xhpeng@cqu.edu.cn

⁵ Department of Mechanical Engineering, Chiba University, 1-33 Yayoi, Inage-ku, Chiba 263-8522, Japan.

and mechanical properties in composites, induced by the change in the distribution of the reinforcement phase, endues FGMs with excellent adaptability to severe loading and environment conditions [Lee (1994)].

The development achieved in recent years implies the great potential of FGMs in a wide range of thermal, biomedical and structural applications [Suresh *et al.* (1998); Watari *et al.* (2004); Reddy (2011); Qiu *et al.* (1999); Tani *et al.* (2001)], and the plate structures made of FGMs have also been widely used in practical engineering. Great progress has been made in the research in the mechanical properties of Functionally graded plates (FGPs), such as buckling, bending and vibration [Feldoman *et al.* (1997); Na and Kim (2006); Aghabaei and Reddy (2009); Altenbach and Eremeyev (2009); Wu and Huang (2009)], crack and thermal fracture [Wang *et al.* (2000); Guo *et al.* (2005)], transient thermal stress [Cheng *et al.* (2000); Vel *et al.* (2002, 2003); Andrew *et al.* (2010)], static and dynamic responses [Zhong *et al.* (2003); Elishakoff *et al.* (2005); Gilhooley *et al.* (2007)], shakedown analysis [Peng *et al.* (2009a, b)], etc.

On the other hand, the concept of FGMs also provides possibilities for optimizing the microstructure parameters of composites to achieve high performance and better utilization of materials [Noda (1990)]. The design of the distributions of the thermal and mechanical properties in FGMs has always been an important topic of research since the concept of FGMs was proposed. It is largely due to the excellent and unique advantages of FGMs, for instance, the combination of the advantages of different materials, the compatibilities between different materials and the good adaptability to various environments [Parashkevova (2004)]. In the past decade, considerable attention has been devoted to FGM representations (Computer-Aided Design), design validation (Computer-Aided Engineering), fabrication (Computer-Aided Manufacturing) and material heterogeneity optimization [Kou (2012)].

In the development of modern structures, optimization is one of the most essential topics in the development of FGMs. Markworth and Saunders (1995) optimized the ceramic/metal composition with certain constraints to maximize or minimize the heat flux through the materials, where the normal thermal stress profiles were calculated and some unusual behavior was found. Ootao *et al.* (1999) optimized the composition in an inhomogeneous hollow sphere with arbitrarily distributed and continuously varying material properties with a neural network approach. Cho and Ha (2002) optimized the volume fraction of Al_2O_3 particles in a Ni/ Al_2O_3 composite to minimize the steady state thermal stress, in which the interior penalty-function method and the golden section method were employed, together with finite differential method for the sensitivity analysis and an appropriate material property estimation for calculating the thermo-mechanical properties in the graded layer. Chen and Tong (2005) presented a systematic numerical technique

to perform sensitivity analysis of coupled thermo-mechanical problems. General formulations were presented based on finite element model by making use of the direct and the adjoint methods.

The initial progress in the analysis of the shakedown of the FG Bree plate, which is subjected to the coupled constant mechanical loading and cyclically varying temperature loading, has been reported in the authors' previous papers [Peng *et al.* (2009a,b); Zheng *et al.* (2012)]. Different from our previous work, in this paper we focus on the optimal distribution of the reinforcement particles in the FG Bree plate, for the purpose to enhance the capability of the FG plate to bear cyclic thermal loading. In order to achieve a more accurate result, we characterize the distribution of the material properties in the thickness of a FG Bree plate with a piecewise exponential distribution [Guo *et al.* (2007)], and the effective mechanical property of a material element of the FG plate is evaluated with a double-inclusion mean field approach [Ju *et al.* (1994)]. Recent developments of "Computational Grains" also enable a direct simulation of a large number of inclusions for composite or FGM, without FEM meshing of inclusions/matrix [Dong, *et al.* (2012a,b; 2013)]. In order to achieve the best shakedown capability of the FG plate, the distribution of reinforcement particles is optimized with the Genetic Algorithm (GA) [Cavalcanti *et al.* (1997); Chen *et al.* (2000); Cho *et al.* (2004); Huang *et al.* (2002); Khalil *et al.* (2004); Kou *et al.* (2006, 2009); Praveen *et al.* (1998); Wadley *et al.* (2003); Williams *et al.* (2005)]. The optimization model for the shakedown of the FG plate is programmed in MATLAB. Two numerical examples are presented to demonstrate the validity of the proposed approach.

2 Constitutive model, static and kinematic shakedown theorems

Assuming small deformation, for initially isotropic and plastically incompressible materials, the constitutive model adopted can be expressed as

$$\boldsymbol{\varepsilon}_{ij} = \boldsymbol{\varepsilon}_{ij}^e + \boldsymbol{e}_{ij}^p + \boldsymbol{\varepsilon}_{ij}^\theta, \quad (1)$$

where $\boldsymbol{\varepsilon}_{ij}$ is strain, $\boldsymbol{\varepsilon}_{ij}^e$, \boldsymbol{e}_{ij}^p and $\boldsymbol{\varepsilon}_{ij}^\theta$ are its elastic, plastic and thermal components, respectively, which are determined with

$$\boldsymbol{\varepsilon}_{ij}^e = \frac{1}{E} [(1 + \nu)\boldsymbol{\sigma}_{ij} - \nu\boldsymbol{\sigma}_{kk}\boldsymbol{\delta}_{ij}], \quad \boldsymbol{\varepsilon}_{ij}^\theta = \alpha(\theta - \theta_0)\boldsymbol{\delta}_{ij}, \quad d\boldsymbol{e}_{ij}^p = d\lambda s_{ij} \quad (2)$$

where E , ν and α are the Young's modulus, the Poisson's ratio and the coefficient of linear expansion, respectively, $\boldsymbol{\sigma}_{ij}$ and s_{ij} are stress and its deviatoric component, θ and θ_0 are temperature and reference temperature, respectively, $\boldsymbol{\delta}_{ij}$ is the Kronecker delta, and [Peng *et al.*, (1996)]

$$d\lambda = d\zeta / [f(\lambda)s_y^0] \quad \text{with} \quad d\zeta = \sqrt{de_{ij}^p de_{ij}^p} \quad (3)$$

s_y^0 is a material constant related to initial yield and $f(\lambda) > 0$ is a function describing the hardening of material. It can be seen that $d\lambda$ is non-negative in any plastic deformation process. The following hardening function is adopted in analysis,

$$f(\lambda) = d - (d - 1)e^{-\beta\lambda}, \quad \text{with } f(0) = 1 \quad \text{and } d \geq 1 \quad (4)$$

It can be seen in Eqs.(3) and (4) that $f(\lambda)$ increases with the development of plastic deformation and tends to an asymptotic value d corresponding to the ultimate strength $\sigma_y = d \cdot \sigma_y^0$ as plastic deformation fully develops when $\lambda \rightarrow \infty$, indicating a saturated state of hardening. Substituting Eq. (3) into Eq. (2)₃ yields the following Mises-type yield condition

$$s_{ij}s_{ij} = [f(\lambda)s_y^0]^2. \quad (5)$$

Introducing the following loading function

$$F(s_{ij}, k) = \sqrt{s_{ij}s_{ij}} - ks_y^0, \quad \text{with } 1 \leq k \leq d \quad (6)$$

It can be seen that any state of stress should satisfy $F(s_{ij}, k) \leq 0$, and $F(s_{ij}, k) = 0$ defines a loading surface.

Given a set of actual stress and hardening states, s_{ij} and k , and a set of allowable stress and hardening states, s_{ij}^*, k^* , which satisfy

$$\begin{aligned} F(s_{ij}, k) &= 0, & 1 \leq k \leq d, \\ F(s_{ij}^*, k^*) &\leq 0, & 1 \leq k^* \leq d \end{aligned} \quad (7)$$

And making use of the following inequality

$$(s_{ij} - s_{ij}^*)de_{ij}^p \geq 0, \quad (8)$$

One can prove that [Peng *et al.* (1993)]

$$(s_{ij}^* - s_{ij})de_{ij}^p \leq s_y^0(k^* - k)d\zeta. \quad (9)$$

2.1 Static Shakedown Theorem [Peng *et al.* (2009a)]

If there exist a time-independent residual stress field $\bar{\rho}_{ij}$ and a time-independent field k^* such that for all the load variations within a given load domain Ω , the following condition holds

$$F(s_{ij}^E + \bar{\rho}_{ij}, k^*) \leq 0 \quad (10)$$

then the total energy dissipated in any allowable load path is bounded.

In Ineq.(10), s_{ij}^E is the purely elastic solution of the deviatoric stress determined by external loads and $1 \leq k^* \leq d$.

2.2 Kinematic Shakedown Theorem [Peng et al. (2009a)]

If there exist over a certain time interval (t_1, t_2) , a history of load resulting in a history of purely elastic stress $s_{ij}^E(\mathbf{x}, t)$, and a history of plastic strain $\bar{e}_{ij}(\mathbf{x}, t)$ resulting in a kinematically admissible increment such that

$$\Delta \bar{e}_{ij}(\mathbf{x}) = \bar{e}_{ij}(\mathbf{x}, t_2) - \bar{e}_{ij}(\mathbf{x}, t_1) = \frac{1}{2}(\Delta \bar{u}_{i,j} + \Delta \bar{u}_{j,i}) \quad (11)$$

with $\Delta \bar{u}_i = 0$ on S_u (the boundary where displacement is prescribed), and if shake-down occurs in the given structure, the condition as Ineq. (12) should be satisfied for all kinematically admissible plastic strain cycles.

$$\int_{t_1}^{t_2} \int_V s_{ij}^E(\mathbf{x}, t) \dot{\bar{e}}_{ij}(\mathbf{x}, t) dV dt \leq \int_{t_1}^{t_2} \int_V D(\dot{\bar{e}}_{ij}(\mathbf{x}, t)) dV dt \quad (12)$$

In Ineq.(12),

$$D(\dot{\bar{e}}_{ij}(\mathbf{x}, t)) = \bar{s}_{ij}(\mathbf{x}, t) \dot{\bar{e}}_{ij}(\mathbf{x}, t) \quad (13)$$

is a dissipation function.

The following relationship can be obtained for practical application by substituting Eq.(2)₃ and Eq.(3) into Ineq. (12) by following the definition by König (1987),

$$\int_V d \cdot s_y^0 \Delta \bar{\zeta} dV - \sum_{k=1}^m \int_V \alpha_k(\mathbf{x}) J_k(\mathbf{x}) dV \geq 0 \quad (14)$$

where

$$\Delta \bar{\zeta} = \|\Delta \bar{e}_{ij}\|, \quad J_k(\mathbf{x}) = s_{ij}^E(\mathbf{x}) \Delta \bar{e}_{ij}(\mathbf{x}), \quad \alpha_k = \begin{cases} \beta_k^+ & \text{if } J_k(\mathbf{x}) > 0 \\ \beta_k^- & \text{if } J_k(\mathbf{x}) < 0 \end{cases} \quad (15)$$

and a set of inequalities $\beta_k^- \leq \beta_k \leq \beta_k^+$ ($k=1, 2, \dots, m$) defines the domain Ω of loads.

3 Optimal model

3.1 The Bree plate

A plate (Figure 1) of thickness h is subjected to loads (P_x, P_y) per unit length in two mutually orthogonal directions. The surfaces of the plate are subjected to temperatures θ_2 and θ_1 which vary cyclically, as shown in Figure 1. The cycle time Δt is assumed large compared with characteristic heat conduction time, and the change, between θ_0 (a reference temperature) and $\theta_0 + \Delta \bar{\theta}$, is assumed to take place sufficiently slowly for steady state conditions of prevail. The strain ε_x and ε_y are assumed to be uniform throughout the thickness of the plate. This problem is a simulation of the behavior of a thin walled tube, in the context of a nuclear fuel can design problem by Bree (1967) for homogeneous material and perfect plasticity.

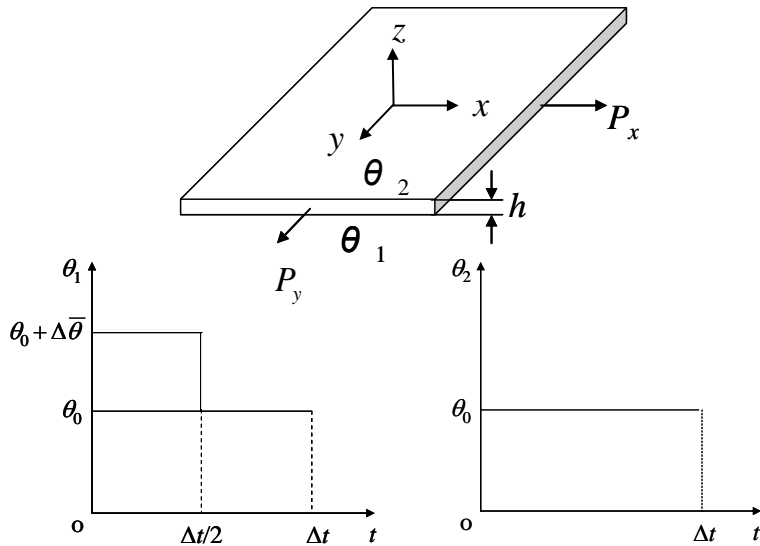


Figure 1: The Bree plate.

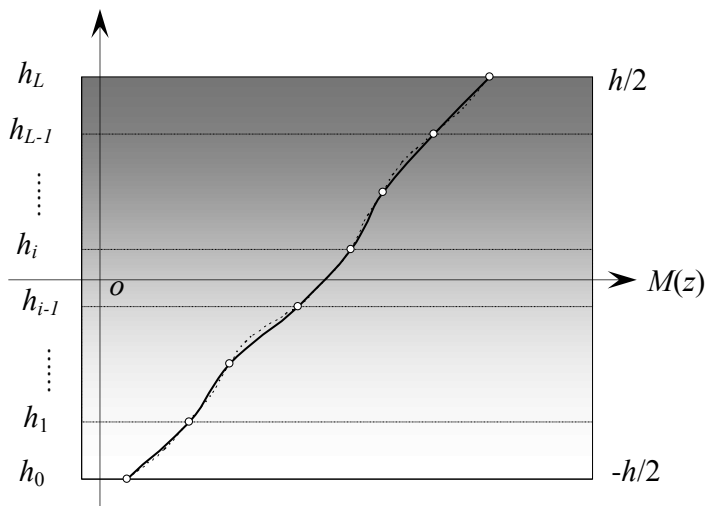


Figure 2: Piecewise-exponential distribution model for FG plate with arbitrarily distributed properties.

3.2 PWED model and material properties

The piece-wise exponential distribution model (PWED model) [Guo *et al.* (2007)] is adopted for the distribution of the material properties in an FG plate, as shown in Figure 2. The plate is assumed to be divided into L parallel layers in the direction of thickness, in each of which the thermal-mechanical properties vary exponentially in the direction of thickness. By this way, the actual thermal-material properties of the plate can be approximated with a set of exponential functions. At both surfaces of a layer the properties are identical with the actual properties of the material. Therefore, the properties of an FG plate can be approximated with sufficient accuracy if the thickness of each layer is sufficiently small.

The plate of thickness h is assumed to be divided into L parallel layers, each of which is marked with subscript i ($i = 1, 2, \dots, L$) counting from the bottom surface of the plate, the i -th layer is located between $z = h_{i-1}$ and $z = h_i$ and at the bottom surface $h_0 = -h/2$, while at the top surface $h_L = h/2$. Suppose $f_M(z)$ is the real distribution of a thermal/mechanical property in a layer, we can approximate $f_M(z)$ with $M(z)$, i.e.,

$$M(z) \approx f_M(z). \quad (16)$$

We further assume

$$M_i(z) = A_{M_i} e^{\beta_{M_i} z}, \quad i = 1, 2, \dots, L, \quad h_{i-1} \leq z \leq h_i \quad (17a)$$

where

$$\begin{cases} M_i(h_{i-1}) = f_M(h_{i-1}) \\ M_i(h_i) = f_M(h_i) \end{cases} \quad i = 1, 2, \dots, L \quad (17b)$$

Given a set of actual values of a thermal/mechanical property, $f_M(h_i)$, $i = 1, 2, \dots, L$, for each segment A_{M_i} and β_{M_i} can be solved from Eqs.(17a,b) as

$$A_{M_i} = f_M(h_i) \left[\frac{f_M(h_i)}{f_M(h_{i-1})} \right]^{-\frac{h_i}{h_i - h_{i-1}}}, \quad \beta_{M_i} = \frac{1}{h_i - h_{i-1}} \ln \left[\frac{f_M(h_i)}{f_M(h_{i-1})} \right] \quad (18)$$

where M can be replaced respectively with the Young's modulus E , the coefficient of thermal expansion α , thermal conductivity λ , and yield stress σ_y^0 , etc., therefore,

$$E_i(z) = A_{E_i} e^{\beta_{E_i} z}, \begin{cases} A_{E_i} = f_E(h_{i-1}) \left[\frac{f_E(h_i)}{f_E(h_{i-1})} \right]^{\frac{-h_{i-1}}{h_i - h_{i-1}}} \\ \beta_{E_i} = \frac{1}{h_i - h_{i-1}} \ln \left[\frac{f_E(h_i)}{f_E(h_{i-1})} \right] \end{cases}, h_{i-1} \leq z \leq h_i, i = 1, 2, \dots, L \quad (19)$$

$$\alpha_i(z) = A_{\alpha_i} e^{\beta_{\alpha_i} z}, \begin{cases} A_{\alpha_i} = f_\alpha(h_{i-1}) \left[\frac{f_\alpha(h_i)}{f_\alpha(h_{i-1})} \right]^{\frac{-h_{i-1}}{h_i - h_{i-1}}} \\ \beta_{\alpha_i} = \frac{1}{h_i - h_{i-1}} \ln \left[\frac{f_\alpha(h_i)}{f_\alpha(h_{i-1})} \right] \end{cases}, h_{i-1} \leq z \leq h_i, i = 1, 2, \dots, L \quad (20)$$

$$\lambda_i(z) = A_{\lambda_i} e^{\beta_{\lambda_i} z}, \begin{cases} A_{\lambda_i} = f_\lambda(h_{i-1}) \left[\frac{f_\lambda(h_i)}{f_\lambda(h_{i-1})} \right]^{\frac{-h_{i-1}}{h_i - h_{i-1}}} \\ \beta_{\lambda_i} = \frac{1}{h_i - h_{i-1}} \ln \left[\frac{f_\lambda(h_i)}{f_\lambda(h_{i-1})} \right] \end{cases}, h_{i-1} \leq z \leq h_i, i = 1, 2, \dots, L \quad (21)$$

$$\sigma_{y_i}^0(z) = A_{y_i} e^{\beta_{y_i} z}, \begin{cases} A_{y_i} = f_y(h_{i-1}) \left[\frac{f_y(h_i)}{f_y(h_{i-1})} \right]^{\frac{-h_{i-1}}{h_i - h_{i-1}}} \\ \beta_{y_i} = \frac{1}{h_i - h_{i-1}} \ln \left[\frac{f_y(h_i)}{f_y(h_{i-1})} \right] \end{cases}, h_{i-1} \leq z \leq h_i, i = 1, 2, \dots, L \quad (22)$$

Considering that the variation of the Poisson's ratio in each layer is insignificant and in order to simplify the analysis, we assume the Poisson's ratio in each layer is a constant taking the mean of the Poisson's ratio over the thickness, i.e.,

$$v_i = [v(h_{i-1}) + v(h_i)]/2, \quad i = 1, 2, \dots, L \quad (23)$$

If the volume fraction of particles at h_i is $\xi(h_i)$, then $f_E(h_i)$, $f_\alpha(h_i)$ and $f_\lambda(h_i)$ can be obtained as [Ju *et al.* (1994); Shen (1998)]

$$f_E(h_i) = \frac{9K(h_i)\mu(h_i)}{3K(h_i) + \mu(h_i)} \quad (24)$$

$$v(h_i) = \frac{3K(h_i) - 2\mu(h_i)}{6K(h_i) + 2\mu(h_i)} \quad (25)$$

$$f_{\alpha}(h_i) = \alpha_m + \frac{(1/K(h_i) - 1/K_m)(\alpha_c - \alpha_m)}{1/K_c - 1/K_m}, \quad (26)$$

$$f_{\lambda}(h_i) = \lambda_m \left[1 + \frac{3\xi(h_i)(\lambda_c/\lambda_m - 1)}{3 - [1 - \xi(h_i)](\lambda_c/\lambda_m - 1)} \right] \quad (27)$$

where

$$K(h_i) = K_m \left\{ 1 + \frac{30\xi(h_i)(1 - \nu_m)[3\gamma_1(h_i) + 2\gamma_2(h_i)]}{3\alpha' + 2\beta - 10\xi(h_i)(1 + \nu_m)[3\gamma_1(h_i) + 2\gamma_2(h_i)]} \right\} \quad (28)$$

$$\mu(h_i) = \mu_m \left\{ 1 + \frac{30\xi(h_i)(1 - \nu_m)\gamma_2(h_i)}{\beta - 4\xi(h_i)(5 - 5\nu_m)\gamma_2(h_i)} \right\} \quad (29)$$

$$\alpha' = 2(5\nu_m - 1) + 10(1 - \nu_m) \left(\frac{K_m}{K_c - K_m} - \frac{\mu_m}{\mu_c - \mu_m} \right), \quad (30)$$

$$\beta = 2(4 - 5\nu_m) + 15(1 - \nu_m) \frac{\mu_m}{\mu_c - \mu_m};$$

$$\gamma_1(h_i) = \frac{5\xi(h_i)}{4\beta^2} \left[-5\nu_m^2 + 2\nu_m - 2 - \frac{4\alpha'(1 - 2\nu_m)(1 + \nu_m)}{3\alpha' + 2\beta} \right] \quad (31)$$

$$\gamma_2(h_i) = \frac{1}{2} + \frac{5\xi(h_i)}{8\beta^2} \left[5\nu_m^2 - 11\nu_m + 11 - \frac{3\alpha'(1 - 2\nu_m)(1 + \nu_m)}{3\alpha' + 2\beta} \right]$$

Here the subscript “m” and “c” denote matrix and inclusion, respectively; K_m , K_c and K are the bulk moduli of the matrix, the inclusion, and the composite, respectively; μ_m , μ_c and μ are shear moduli of the matrix, the inclusion, and the composite, respectively.

Combining the mean field scheme [Ju *et al.* (1994)] and the constitutive model mentioned in section 2, one can obtain $f_y(h_i)$.

3.3 Distribution of temperature

Assuming steady-state heat transfer, the distribution of the temperature in a structure can be described with the following equation of heat conduction, without considering source heat,

$$\nabla \cdot \{ \lambda(\mathbf{x}) \nabla \theta \} = 0 \quad (32)$$

For uniaxial heat transfer, as shown in Figure 3, Eq. (32) can be simplified as

$$\frac{d}{dz} \left\{ \lambda(z) \frac{d\theta}{dz} \right\} = 0 \quad (33)$$

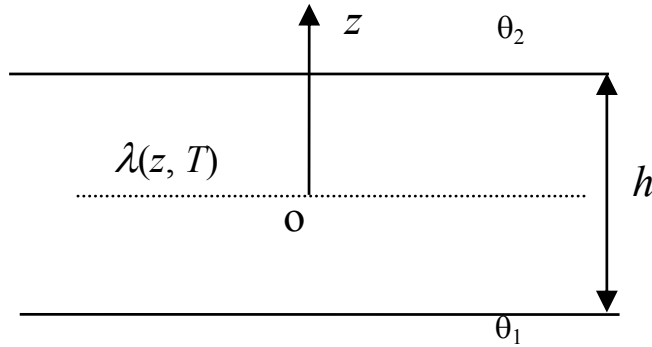


Figure 3: Heat transfer in Bree plate

Making the boundary condition shown in Figure 3, we obtain

$$\theta(z) = \theta_2 + (\theta_1 - \theta_2) \left[\int_z^{h/2} \frac{1}{\lambda(z')} dz' / \int_{-h/2}^{h/2} \frac{1}{\lambda(z)} dz \right]. \quad (34)$$

Letting $\Delta\tilde{\theta} = \theta_1 - \theta_2$, $\Delta\theta(z) = \theta(z) - \theta_2$, Eq. (34) can be rewritten as

$$\Delta\theta(z) = \Delta\tilde{\theta} \left[1 - \int_{-h/2}^z \frac{1}{\lambda(z')} dz / \int_{-h/2}^{h/2} \frac{1}{\lambda(z)} dz \right] \quad (35a)$$

For the distribution of the temperature in the Bree plate shown in Figure 1,

$$\Delta\tilde{\theta} = \begin{cases} \Delta\tilde{\theta} & n\Delta t \leq t \leq (n+0.5)\Delta t \\ 0 & (n+0.5)\Delta t \leq t \leq (n+1)\Delta t \end{cases}, \quad n = 0, 1, 2, \dots \quad (35b)$$

Substituting Eq.(21) into Eq.(35a), there have been

$$\int_{-h/2}^z \frac{1}{\lambda(z')} dz' = \frac{e^{-\beta\lambda_i h_{i-1}} - e^{-\beta\lambda_i z}}{A\lambda_i \beta\lambda_i} + \sum_{j=1}^{i-1} \frac{e^{-\beta\lambda_j h_{j-1}} - e^{-\beta\lambda_j h_j}}{A\lambda_j \beta\lambda_j}, \quad i = 1, 2, \dots, L \quad (36a)$$

$$\int_{-h/2}^{h/2} \frac{1}{\lambda(z)} dz = \sum_{i=1}^L \frac{e^{-\beta\lambda_i h_{i-1}} - e^{-\beta\lambda_i h_i}}{A\lambda_i \beta\lambda_i} \quad (36b)$$

And then $\Delta\theta_i(z)$ can be obtained as

$$\Delta\theta_i(z) = \Delta\tilde{\theta} \left(A\theta_i + B\theta_i e^{-\beta\lambda_i z} \right) \quad (37a)$$

Here

$$A_{\theta_i} = 1 - \left(\frac{e^{-\beta_{\lambda_i} h_{i-1}}}{A_{\lambda_i} \beta_{\lambda_i}} + \sum_{j=1}^{i-1} \frac{e^{-\beta_{\lambda_j} h_{j-1}} - e^{-\beta_{\lambda_j} h_j}}{A_{\lambda_j} \beta_{\lambda_j}} \right) / \left(\sum_{k=1}^L \frac{e^{-\beta_{\lambda_k} h_{k-1}} - e^{-\beta_{\lambda_k} h_k}}{A_{\lambda_k} \beta_{\lambda_k}} \right),$$

$$i = 1, 2, \dots, L \quad (37b)$$

$$B_{\theta_i} = \frac{1}{A_{\lambda_i} \beta_{\lambda_i}} / \left(\sum_{k=1}^L \frac{e^{-\beta_{\lambda_k} h_{k-1}} - e^{-\beta_{\lambda_k} h_k}}{A_{\lambda_k} \beta_{\lambda_k}} \right), \quad i = 1, 2, \dots, L \quad (37c)$$

3.4 Purely elastic solution

For the FG Bree plate, we will be concerned with the solution when the displacement in y -direction is fixed, i.e., $\varepsilon_y = 0$, for simplicity. In this case, we need not be concerned with the yield condition in y -direction [Bree (1967)]. The components of the strain in the plate subjected to stress σ_x, σ_y can be expressed as

$$\varepsilon_x - \alpha(z) \Delta\theta(z) = (\sigma_x - \nu \sigma_y) / E(z) \quad (38a)$$

$$\varepsilon_y - \alpha(z) \Delta\theta(z) = (\sigma_y - \nu \sigma_x) / E(z) \quad (38b)$$

where $\Delta\theta_i(z)$ is the temperature change at z . Keeping in mind that $\varepsilon_y = 0$, it can be solved from Eq. (38) that

$$\sigma_x = E(z) [\varepsilon_x - \alpha(z) (1 + \nu) \Delta\theta(z)] / (1 - \nu^2). \quad (39)$$

(1) Purely elastic solution of the stress distribution σ_P caused by P_x

When P_x is applied individually, i.e., $\Delta\theta(z) = 0$, the equilibrium in x -direction gives

$$\int_{-h/2}^{h/2} \sigma_P dz = \int_{-h/2}^{h/2} [E(z) / (1 - \nu^2)] \varepsilon_x dz = P_x. \quad (40a)$$

Substituting Eq. (39) and $\Delta\theta(z) = 0$ into Eq. (40a), one obtains

$$\varepsilon_x = \varepsilon_0 = P_x / \int_{-h/2}^{h/2} [E(z) / (1 - \nu^2)] dz. \quad (40b)$$

Keeping in mind that ν is treated as a constant (Eq. (23)) and using Eq. (39), we obtain the purely elastic solution of the stress distribution σ_P caused by P_x as

$$\sigma_P(z) = \left[E(z) / \int_{-h/2}^{h/2} E(z) dz \right] P_x \quad (41a)$$

Making use of the PWED model, the denominator on the RHS of Eq. (41a) can further be expressed as

$$\int_{-h/2}^{h/2} E(z) dz = \sum_{i=1}^L \int_{h_{i-1}}^{h_i} E_i(z) dz \approx \sum_{i=1}^L \int_{h_{i-1}}^{h_i} A_{E_i} e^{\beta_{E_i} z} dz = \sum_{i=1}^L \frac{A_{E_i}}{\beta_{E_i}} \left(e^{\beta_{E_i} h_i} - e^{\beta_{E_i} h_{i-1}} \right) \quad (41b)$$

Thus, Eq. (41a) can be expressed in the following discrete form

$$\sigma_{pi}(z) = \left\{ A_{E_i} e^{\beta_{E_i} z} / \left[\sum_{k=1}^L \frac{A_{E_k}}{\beta_{E_k}} \left(e^{\beta_{E_k} h_k} - e^{\beta_{E_k} h_{k-1}} \right) \right] \right\} P_x, \quad i = 1, 2, \dots, L \quad (42)$$

(2) Purely elastic solution of the stress distribution σ_θ caused by $\Delta\bar{\theta}$

When $\Delta\bar{\theta}$ is applied individually, one has the following condition of equilibrium

$$\int_A \sigma_x dA = 0. \quad (43)$$

Keeping in mind that

$$\varepsilon_x = \varepsilon_0 \quad (44)$$

And substituting Eq. (39) into Eq. (43) yields

$$\varepsilon_x = \varepsilon_0 = (1 + \nu) \int_{-h/2}^{h/2} \alpha(z) E(z) \Delta\theta(z) dz / \int_{-h/2}^{h/2} E(z) dz \quad (45)$$

Combining Eq. (45) with Eq. (39), the distribution of the thermal stress can be determined as

$$\sigma(z, \Delta\bar{\theta}) = \sigma_x|_{P_x=0} = \frac{E(z)}{1 - \nu} \left[\int_{-h/2}^{h/2} \alpha(z) E(z) \Delta\theta(z) dz / \int_{-h/2}^{h/2} E(z) dz - \alpha(z) \Delta\theta(z) \right] \quad (46a)$$

Making use of the PWED model, we obtain the following discrete form

$$\sigma_{\theta i}(z, \Delta\bar{\theta}) = \frac{E_i(z)}{1 - \nu} \left[\frac{\sum_{k=1}^L \int_{h_{k-1}}^{h_k} \alpha_k(z) E_k(z) \Delta\theta_k(z) dz}{\sum_{k=1}^L \int_{h_{k-1}}^{h_k} E_k(z) dz} - \alpha_i(z) \Delta\theta_i(z) \right], \quad i = 1, 2, \dots, L \quad (46b)$$

Substituting Eqs.(19) - (21) and Eq.(37a) into Eq.(46b), we can obtain

$$\sigma_{\theta i}(z, \Delta \bar{\theta}) = \Delta \bar{\theta} f_i(z), \quad i = 1, 2, \dots, L \quad (47a)$$

where

$$f_i(z) = \frac{A_{E_i} e^{\beta_{E_i} z}}{1 - \nu} \left[\frac{\sum_{k=1}^L \int_{h_{k-1}}^{h_k} A_{\alpha_k} A_{E_k} e^{(\beta_{E_k} + \beta_{\alpha_k})z} (A_{\theta_k} + B_{\theta_k} e^{-\beta_{\lambda_k} z}) dz}{\sum_{k=1}^L \int_{h_{k-1}}^{h_k} A_{E_k} e^{\beta_{E_k} z} dz} - A_{\alpha_i} e^{\beta_{\alpha_i} z} (A_{\theta_i} + B_{\theta_i} e^{-\beta_{\lambda_i} z}) \right] \quad (47b)$$

Compared with Eq. (43), there is $\sum_{i=1}^L \int_{h_{i-1}}^{h_i} f_i(z) dz = 0$. Here, the first term in the square bracket on the right side of Eq. (47b) can be expressed as

$$\begin{aligned} & \frac{\sum_{i=1}^L \int_{h_{i-1}}^{h_i} A_{\alpha_i} A_{E_i} e^{(\beta_{E_i} + \beta_{\alpha_i})z} (A_{\theta_i} + B_{\theta_i} e^{-\beta_{\lambda_i} z}) dz}{\sum_{i=1}^L \int_{h_{i-1}}^{h_i} A_{E_i} e^{\beta_{E_i} z} dz} \\ &= \frac{\sum_{i=1}^L A_{\alpha_i} A_{E_i} \left[A_{\theta_i} \frac{e^{(\beta_{E_i} + \beta_{\alpha_i})h_i} - e^{(\beta_{E_i} + \beta_{\alpha_i})h_{i-1}}}{\beta_{E_i} + \beta_{\alpha_i}} + B_{\theta_i} \frac{e^{(\beta_{E_i} + \beta_{\alpha_i} - \beta_{\lambda_i})h_i} - e^{(\beta_{E_i} + \beta_{\alpha_i} - \beta_{\lambda_i})h_{i-1}}}{\beta_{E_i} + \beta_{\alpha_i} - \beta_{\lambda_i}} \right]}{\sum_{i=1}^L \frac{A_{E_i}}{\beta_{E_i}} (e^{\beta_{E_i} h_i} - e^{\beta_{E_i} h_{i-1}})} \end{aligned} \quad (47c)$$

3.5 Static shakedown analysis

The analysis for the shakedown of the Bree plate includes the determination of the boundary of initial yield, the boundary between the areas of shakedown and incremental collapse, and the boundary between the areas of shakedown and reversed plasticity.

The plate contains two parts, in one part $f_i(z) \leq 0$ and in the other part $f_i(z) \geq 0$. For the thermal and mechanical loading shown in Figure 1, we can obtain the following shakedown boundaries.

(1) Initial yield

No plastic deformation takes place on the condition that

$$\sigma_{P_i}(z) + \sigma_{\theta i}(z, \Delta \bar{\theta}) \leq \sigma_{yi}^0(z), \quad \text{for } f_i(z) \geq 0 \quad (48a)$$

$$\begin{aligned} & \sigma_{P_i}(z) + \sigma_{\theta i}(z, \Delta \bar{\theta}) \geq -\sigma_{yi}^0(z) \quad \text{and} \quad \sigma_{P_i}(z) \leq \sigma_{yi}^0(z). \\ & \text{for } f_i(z) \leq 0 \quad i = 1, 2, \dots, L \end{aligned} \quad (48b)$$

(2) Static shakedown boundaries

Suppose there are a time-independent residual stress field $\bar{\rho}_{xi}(z)$ and a time-independent field k^* ($1 \leq k^* \leq d$), the shakedown will occur to the plate if the following condition is satisfied in one temperature change cycle

$$\sigma_{Pi}(z) + \sigma_{\theta i}(z, \Delta\bar{\theta}) + \bar{\rho}_{xi}(z) \leq \sigma_{yi}(z), \quad \text{for } f_i(z) \geq 0 \quad i = 1, 2, \dots, L \quad (49a)$$

$$\sigma_{Pi}(z) + \sigma_{\theta i}(z, \Delta\bar{\theta}) + \bar{\rho}_{xi}(z) \geq -\sigma_{yi}(z), \quad \text{for } f_i(z) \leq 0 \quad i = 1, 2, \dots, L \quad (49b)$$

$$\sigma_{Pi}(z) + \bar{\rho}_{xi}(z) \geq -\sigma_{yi}(z), \quad \text{for } f_i(z) \geq 0 \quad i = 1, 2, \dots, L \quad (49c)$$

$$\sigma_{Pi}(z) + \bar{\rho}_{xi}(z) \leq \sigma_{yi}(z). \quad \text{for } f_i(z) \leq 0 \quad i = 1, 2, \dots, L \quad (49d)$$

where $\sigma_{yi}(z) = k^* \sigma_{yi}^0(z)$ and $k^* = d$.

The shakedown boundaries of the plate contain two parts: the boundary between the area of shakedown and that of incremental collapse, and the boundary between the area of shakedown and that of reversed plasticity.

(a) Shakedown boundary corresponding to reversed plasticity

It can be obtained from Ineq. (49) that

$$\sigma_{\theta i}(z, \Delta\bar{\theta}) \leq 2\sigma_{yi}(z), \quad \text{for } f_i(z) \geq 0 \quad i = 1, 2, \dots, L \quad (50a)$$

$$\sigma_{\theta i}(z, \Delta\bar{\theta}) \geq -2\sigma_{yi}(z). \quad \text{for } f_i(z) \leq 0 \quad i = 1, 2, \dots, L \quad (50b)$$

The equality of both sides of anyone in Ineq. (50) at any point in the cross section implies the equality of both sides of Ineqs. (49a) and (49c), or the equality of Ineqs. (49b) and (49d), indicating that reversed plasticity occurs at this point in the cross section.

(b) Shakedown boundary corresponding to incremental collapse

Making use of the given time-independent residual stress field $\bar{\rho}_{xi}(z)$ and noticing that $\Delta\bar{\theta} = \Delta\bar{\theta}$ as $n\Delta t \leq t \leq (n + 0.5)\Delta t$, Ineqs.(49a,b) can be rewritten in this duration as

$$\sigma_{Pi}(z) + \sigma_{\theta i}(z, \Delta\bar{\theta}) + \bar{\rho}_{xi}(z) = \sigma_{yi}(z), \quad \text{for } f_i(z) \geq 0 \quad i = 1, 2, \dots, L \quad (51a)$$

$$\sigma_{Pi}(z) + \sigma_{\theta i}(z, \Delta\bar{\theta}) + \bar{\rho}_{xi}(z) \geq -\sigma_{yi}(z). \quad \text{for } f_i(z) \leq 0 \quad i = 1, 2, \dots, L \quad (51b)$$

Since $\Delta\bar{\theta} = 0$ as $(n + 0.5)\Delta t \leq t \leq (n + 1)\Delta t$, in this duration Ineqs. (49c, d) will be reduced to

$$\sigma_{Pi}(z) + \bar{\rho}_{xi}(z) \geq -\sigma_{yi}(z), \quad \text{for } f_i(z) \geq 0 \quad i = 1, 2, \dots, L \quad (51c)$$

$$\sigma_{Pi}(z) + \bar{\rho}_{xi}(z) = \sigma_{yi}(z). \quad \text{for } f_i(z) \leq 0 \quad i = 1, 2, \dots, L \quad (51d)$$

Ineq. (51) indicates that at each point in the region where $f_i(z) \geq 0$ of the cross section, the stress $\sigma_+ = \sigma_{P_i}(z) + \sigma_{\theta_i}(z, \Delta\bar{\theta}) + \bar{\rho}_{xi}(z)$ reaches $\sigma_{y_i}(z)$; while at each point in the region where $f_i(z) \leq 0$ of the cross section, the stress $\sigma_- = \sigma_{P_i}(z) + \bar{\rho}_{xi}(z)$ reaches $\sigma_{y_i}(z)$. That is, during $n\Delta t \leq t \leq (n+0.5)\Delta t$, σ_+ in a part of the Bree plate reaches $\sigma_{y_i}(z)$, and during $(n+0.5)\Delta t \leq t \leq (n+1)\Delta t$, σ_- at the in the rest part of the Bree plate reaches $\sigma_{y_i}(z)$. The two parts of the cross section may flow forward alternatively.

3.6 Objective of optimization

To theorize objective function is the key in GA approach. In this paper the objective of the optimization is the maximization of $\Delta\bar{\theta}$ in the FG Bree plate under the condition of shakedown. The temperature $\Delta\bar{\theta}$ can be solved from Ineqs. (50a,b) and Eq. (47a) as

$$\Delta\bar{\theta} \leq 2\sigma_{y_i}(z)/|f_i(z)|, \quad i = 1, 2, \dots, L \quad (52)$$

Eq.(52) can also be expressed as

$$\Delta\bar{\theta}_{\max} = \min(2\sigma_{y_i}(z)/|f_i(z)|), \quad i = 1, 2, \dots, L \quad (53)$$

The objective of the optimization is to find $\Delta\bar{\theta}_{\max}$.

3.7 Variables and constraint of optimization

The objective to be optimized is the distribution of volume fraction of the reinforcement particles in a FG Bree plate. The distribution function is assumed as

$$V_c(z) = \begin{cases} a_1 (-2z/h)^{P_1} & -h/2 \leq z \leq 0 \\ a_2 (2z/h)^{P_2} & 0 \leq z \leq h/2 \end{cases} \quad (54)$$

where $h = 60\text{mm}$ is the thickness of the plate, and the variables to be optimized are a_1, a_2, P_1 and P_2 . The boundaries of these variables are assumed as

$$\text{Opt}_{0.3}: a_1, a_2 \in [0.0, 0.3]; P_1, P_2 \in [0.0, 2]$$

$$\text{Opt}_{0.4}: a_1, a_2 \in [0.0, 0.4]; P_1, P_2 \in [0.0, 3]$$

$$\text{Opt}_{0.5}: a_1, a_2 \in [0.0, 0.5]; P_1, P_2 \in [0.0, 3]$$

The constraint to the optimization is that the gross volume fraction of the reinforcement particles in the plate is 15%, i.e.,

$$\frac{1}{h} \int_{-h/2}^{h/2} V_c(z) dz = 0.15 \quad (55)$$

The shakedown of the plate is determined with Ineqs.(48)-(51), and the best distribution of the volume fraction of the reinforcement particles is obtained by optimization calculation.

3.8 Computing process of GA approach

In this paper, the first important thing is to program subroutines in matlab language about the constraint function and the fitting function which is related to the objective function. The computer process of the optimization is depicted in Figure 4.

The parameters in GA approach are given as follows. The population type is double vector and the population size is 100. The numerical value of generations is 100. The crossover fraction is 0.8 and mutation fraction is 0.01. The constraint function is solved by penalty function method and the penalty factor is 100.

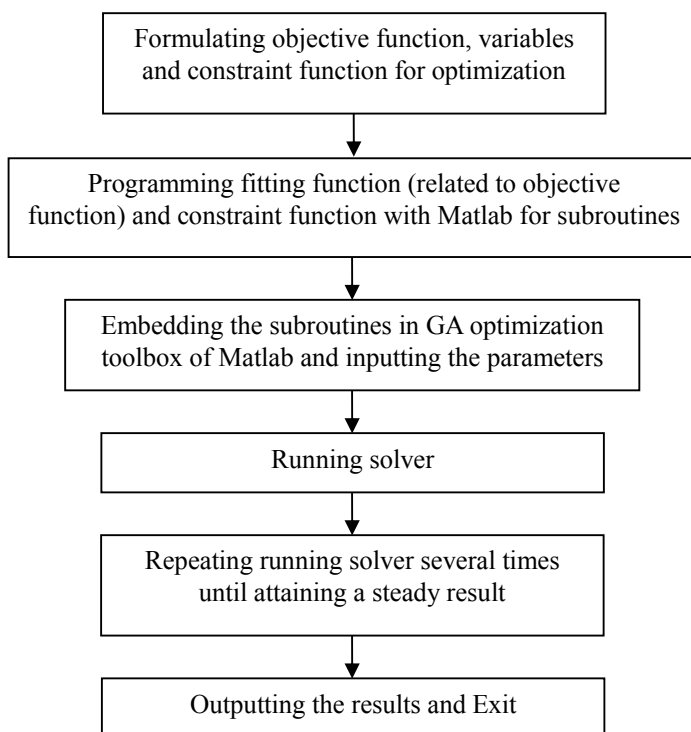


Figure 4: Computer process of the optimization.

4 Numerical examples

4.1 Optimal design of Al/SiC FG Bree plate

The first example is the optimization of an Al/SiC FG Bree plate. The reinforcement phase is SiC, and the total volume fraction of the SiC particles keeps 15% in

the optimization process. The material properties of Al and SiC [Shen (1998)] are listed in Table 1.

Table 1: Material properties of Al and SiC.

	E (GPa)	ν	G (GPa)	α (K^{-1})	λ (W/K.m)	σ_y (MPa)	σ_u (MPa)	d
Al	69.	0.33	25.94	$23.1. \times 10^{-6}$	237	34	79	2.32
SiC	450.	0.17	192.31	$4.7. \times 10^{-6}$	368	—	—	—

The optimal design results of the Al/SiC FG plate are

$$\text{Opt}_{0.3} : \quad V_c(z) = \begin{cases} 0.2048 \left(-\frac{2z}{h}\right)^2 & -h/2 \leq z \leq 0 \\ 0.3 \left(\frac{2z}{h}\right)^{0.2946} & 0 \leq z \leq h/2 \end{cases} \quad (56)$$

$$\text{Opt}_{0.4} : \quad V_c(z) = \begin{cases} 0.2343 \left(-\frac{2z}{h}\right)^{2.2271} & -h/2 \leq z \leq 0 \\ 0.4 \left(\frac{2z}{h}\right)^{0.7591} & 0 \leq z \leq h/2 \end{cases} \quad (57)$$

$$\text{Opt}_{0.5} : \quad V_c(z) = \begin{cases} 0.2932 \left(-\frac{2z}{h}\right)^{2.5931} & -h/2 \leq z \leq 0 \\ 0.5 \left(\frac{2z}{h}\right)^{1.2892} & 0 \leq z \leq h/2 \end{cases} \quad (58)$$

The shakedown boundaries of Al/SiC FG Bree plates, with the volume fraction distribution functions of the SiC particles given above, are shown in Figure 4 with the curves marked with curve Opt_0.3, curve Opt_0.4 and curve Opt_0.5, respectively. For comparison, the shakedown boundaries of the Al/SiC FG plates with the volume fraction distribution functions given in Eqs. (59)-(61) are also shown in Figure 4, respectively, denoted as Linear 1, Linear 2 and Homo_0.15.

$$V_c(z) = 0.3 \left(\frac{1}{2} + \frac{z}{h}\right) \quad (59)$$

$$V_c(z) = 0.3 \left(\frac{1}{2} - \frac{z}{h}\right) \quad (60)$$

$$V_c(z) = 0.15 \quad (61)$$

The distributions of the stress in the plates corresponding to points E₁ through E₆ are shown in Figures 6-11, respectively, where $\bar{\rho}_x$ denotes the residual stress, σ_θ the thermal stress, σ_P the mechanical stress, σ_y the yield strength, σ_+ the stress $\sigma_\theta + \sigma_P + \bar{\rho}_x$ and σ_- the stress $\sigma_P + \bar{\rho}_x$ in the plates.

Figures 6 and 7 show respectively the stress distributions in the Al/SiC FG plates corresponding to the points E₁ (with V_c determined by Eq. (59)) and E₂ (with

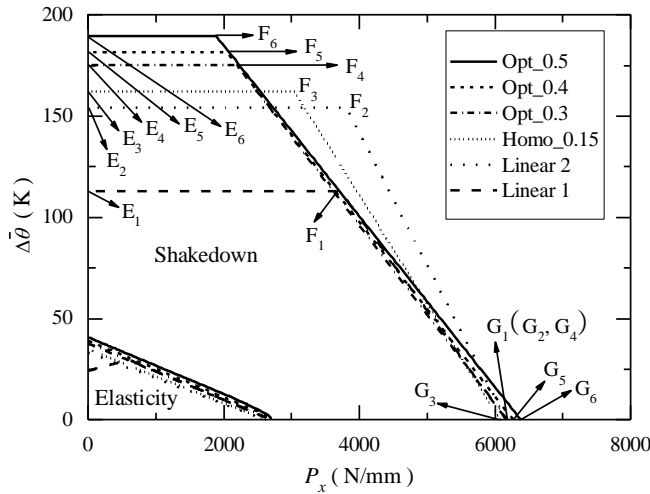


Figure 5: Shakedown area of different Al/SiC FG Bree plate after optimization.

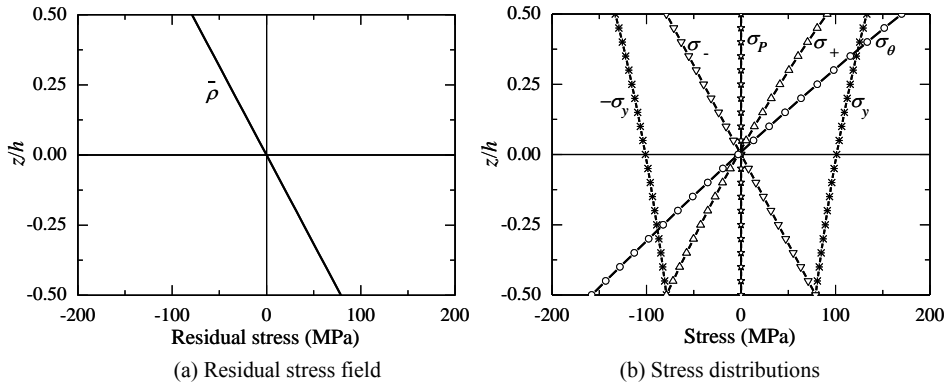


Figure 6: Stress distributions in Al/SiC FG plate corresponding to point E_1 .

V_c determined by Eq.(60)) in Figure 5. It can be seen in Figure 5 that the $\Delta\bar{\theta}$ at E_2 is larger than that at E_1 . The comparison between the stress distributions shown in Figures 6 and 7 indicates that the difference in $\Delta\bar{\theta}$ can be attributed to the difference between the distributions of stress, and the difference between the material properties, for example, the yield strength. One can find in Figure 6 that, the weakest point where both σ_+ and σ_- reach the yield strength, is located at the lower surface of the plate, where the yield strength of the material is the lowest. While in Figure 7 the weakest point, where both σ_+ and σ_- reach the yield strength,

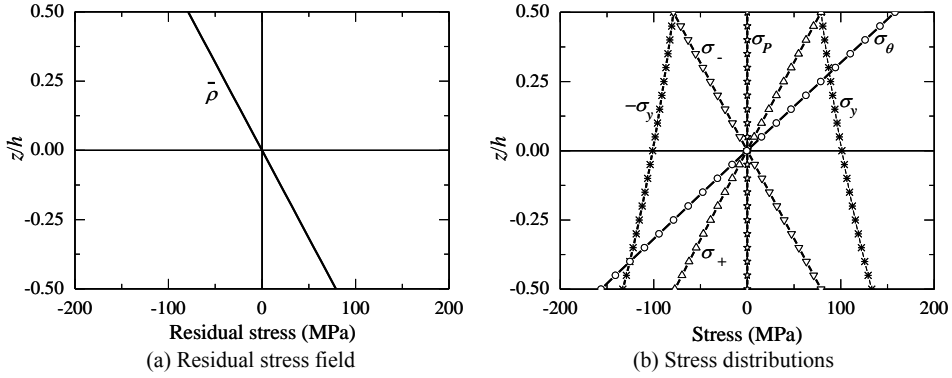


Figure 7: Stress distributions in Al/SiC FG plate corresponding to point E_2 .

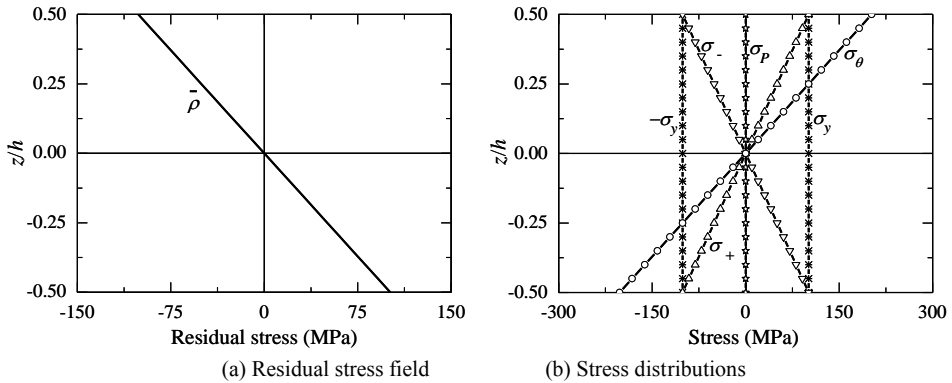


Figure 8: Stress distributions in Al/SiC effective homogeneous plate corresponding to point E_3 .

is located at the upper surface of the plate, where the yield strength of the material is the lowest.

The stress distributions in the plate, corresponding to the point E_3 on the curve marked with Homo_0.15 (Figure 5) are shown in Figure 8, in which the SiC particles distribute uniformly with $V_c = 0.15$ (Eq. (61)). It can be seen that for the residual stress field shown in Figure 8(a), the obtained σ_+ and σ_- reach the yield strength at both the upper and the lower surfaces. The corresponding $\Delta\bar{\theta}$ (Figure 5) is a little larger than that corresponding to E_2 . The comparison between the results corresponding to points E_1 , E_2 and E_3 implies the possibility to achieve a better shakedown boundary by optimizing the distribution of the material properties with a proper distribution of particle volume fraction.

The optimized shakedown boundary corresponding to the distribution of Eq.(56) is given in Figure 5 with the curve marked with Opt_0.3. Given the residual stress field shown in Figure 9(a), the stress distributions at point E₄ are shown in Figure 9(b), where it can be seen that reversed plastic deformation takes place at both the upper and the lower surfaces. Compared with the result at either E₁, E₂ or E₃, the $\Delta\bar{\theta}$ at E₄ of Opt_0.3 increases to some extent.

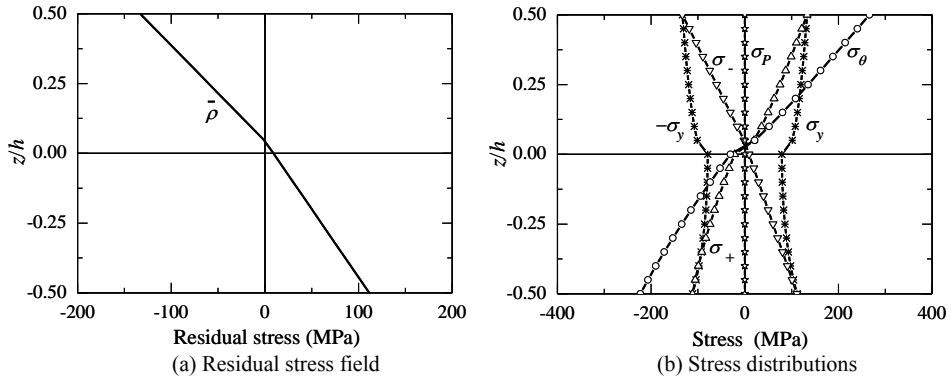


Figure 9: Stress distributions in Al/SiC FG plate corresponding to point E₄.

The optimized shakedown boundary corresponding to the distribution of Eq. (57) is given in Figure 5 with the curve marked with Opt_0.4. Given the residual stress field shown in Figure 10(a), the stress distributions at point E₅ are shown in Figure 10(b), where it can be seen that reversed plastic deformation takes place at both the upper and the lower surfaces. Compared with the result at E₄, the $\Delta\bar{\theta}$ at E₅ in the curve marked with Opt_0.4 increases, which could be attributed to that the maximum particle volume fraction at the upper surface is increased from 0.3 to 0.4, which enhances the capability of the plate to bear the thermal loading.

The optimized shakedown boundary corresponding to the distribution of the particle volume fraction of Eq. (58) is given in Figure 5 with the curve marked with Opt_0.5. Given the residual stress field shown in Figure 11(a), the stress distributions at point E₆ are shown in Figure 11(b), where it can be seen that reversed plastic deformation takes place at both two surface (one is the upper surface, the other one is not the lower surface but a little higher than it). Compared with the result at E₅, the $\Delta\bar{\theta}$ at E₆ in the curve marked with Opt_0.5 further increases, which could be attributed to that the maximum particle volume fraction at the upper surface is increased from 0.4 to 0.5, which further enhances the capability of the plate to bear the thermal loading.

The comparison between the $\Delta\bar{\theta}$ at the points E₁ through E₆ in Figure 5 shows that

the $\Delta\bar{\theta}$ at E_6 , corresponding to the distribution of the particle volume fraction, Eq. (58), is the largest. If the maximum particle volume fraction is limited to 0.5, this $\Delta\bar{\theta}$ can be regarded as $\Delta\bar{\theta}_{\max}$.

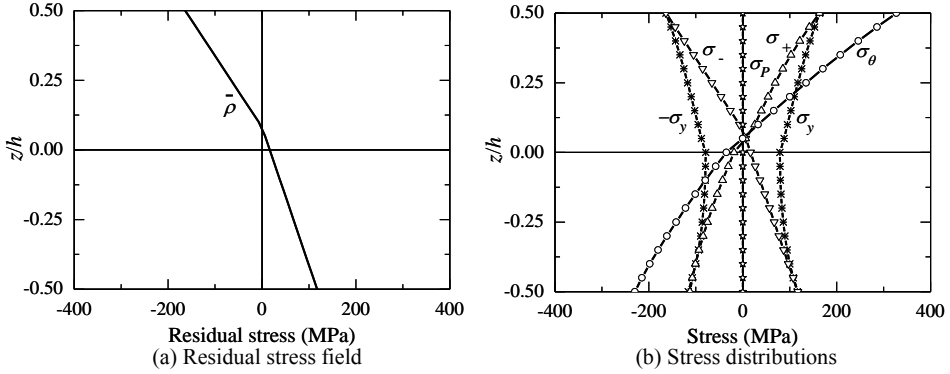


Figure 10: Stress distributions in Al/SiC FG plate corresponding to point E_5 .

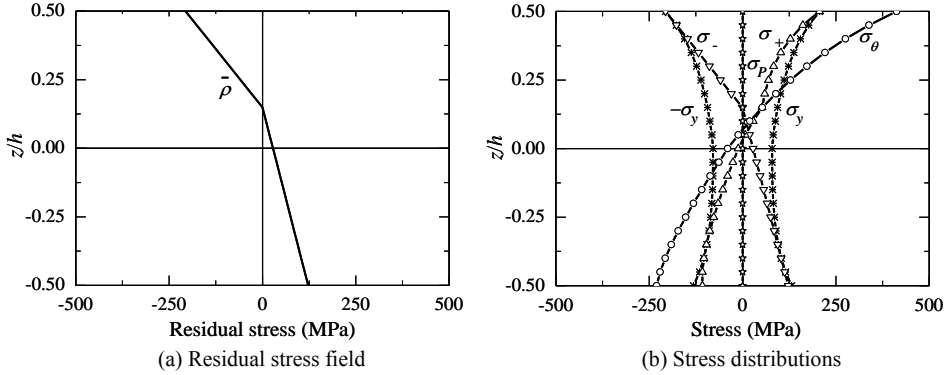


Figure 11: Stress distributions in Al/SiC FG plate corresponding to point E_6 .

4.2 Optimal design of Ti/Si₃N₄ FG Bree plate

In order to further verify the optimal design model, the optimization for shakedown capability of a Ti/Si₃N₄ FG Bree plate is performed, in which the Si₃N₄ particles are the reinforcement phase. Material constants of Ti and Si₃N₄ [Cho et al. (2004)] are listed in Table 2.

We also assume three classes of the Ti/Si₃N₄ FG Bree plates, of which the distribution of the Si₃N₄ particle volume function is described with Eq. (54), where a_1, P_1

Table 2: Material constants of Ti and Si₃N₄.

	E (GPa)	ν	G (GPa)	α (K ⁻¹)	λ (W/K.m)	σ_y (MPa)	σ_u (MPa)	d
Ti	117.	0.32	44.32	$8.6. \times 10^{-6}$	21.9	175	175	1.
Si ₃ N ₄	310.	0.27	122.05	$3.3. \times 10^{-6}$	30.	—	—	—

and a_2 , P_2 are the parameters to be optimized. If the average particle volume is limited to 0.15, and the maximum local particle volume fractions of the three classes are 0.3 (Class 1), 0.4 (Class 2) and 0.5 (Class 3), respectively, the corresponding shakedown boundaries are shown in Figure 12 with the curves marked with Opt_0.3, o Opt_0.4 and Opt_0.5, respectively. With the optimized a_1 , P_1 and a_2 , P_2 , the three classes distribution functions can be expressed as

$$\text{Opt}_{0.3}: V_c(z) = \begin{cases} 0.2175 \left(-\frac{2z}{h}\right)^{1.9999} & -h/2 \leq z \leq 0 \\ 0.3 \left(\frac{2z}{h}\right)^{0.3188} & 0 \leq z \leq h/2 \end{cases} \quad (62)$$

$$\text{Opt}_{0.4}: V_c(z) = \begin{cases} 0.2877 \left(-\frac{2z}{h}\right)^{2.4024} & -h/2 \leq z \leq 0 \\ 0.4 \left(\frac{2z}{h}\right)^{0.8566} & 0 \leq z \leq h/2 \end{cases} \quad (63)$$

$$\text{Opt}_{0.5}: V_c(z) = \begin{cases} 0.3404 \left(-\frac{2z}{h}\right)^{2.1676} & -h/2 \leq z \leq 0 \\ 0.5 \left(\frac{2z}{h}\right)^{1.5968} & 0 \leq z \leq h/2 \end{cases} \quad (64)$$

For comparison, the shakedown boundaries of Ti/Si₃N₄ FG plates with the particle volume fraction distribution functions of Eqs.(59)-(61) are also given in Figure 12 with the curves marked with Linear 1, Linear 2 and Homo_0.15 respectively.

Figure 13 show the stress distributions in the FG plate corresponding to point E₁ on the curve marked as Linear 1 in Figure 13. Figure 14 shows the stress distributions in the FG plate corresponding to point E₂ on the curve marked as Linear 2 in Figure 11. The results shown in Figure 13 and Figure 14 are respectively similar to that in Figure 6 and Figure 7.

Then, the shakedown of the equivalent homogenous plate is analyzed in the same way as numerical example 1, and the boundary which is marked as Homo_0.15 is shown in Figure 12. Stress distributions corresponding to point E₃ are shown in Figure 15.

Be similar to the numerical example of Al/SiC FG plate, the optimization of Ti/Si₃N₄ FG plate is given. The results of optimal volume fraction distribution functions of Si₃N₄ have been given as Eqs. (62)-(64), and the shakedown boundaries of corresponding FG plates have been shown as Opt_0.3, Opt_0.4 and Opt_0.5 in Figure

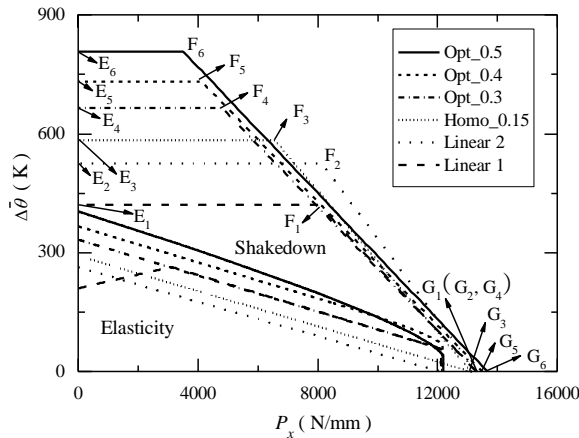


Figure 12: Shakedown area of different Ti/Si₃N₄ FG Bree plate after optimization.

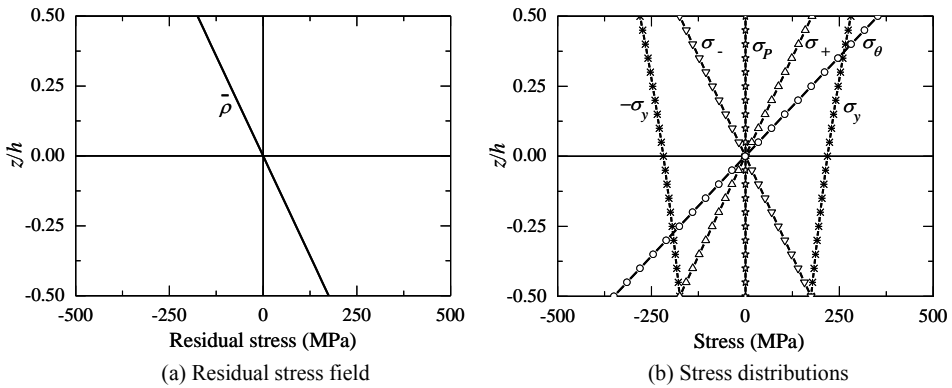


Figure 13: Stress distributions in Ti/Si₃N₄ FG plate corresponding to point E₁.

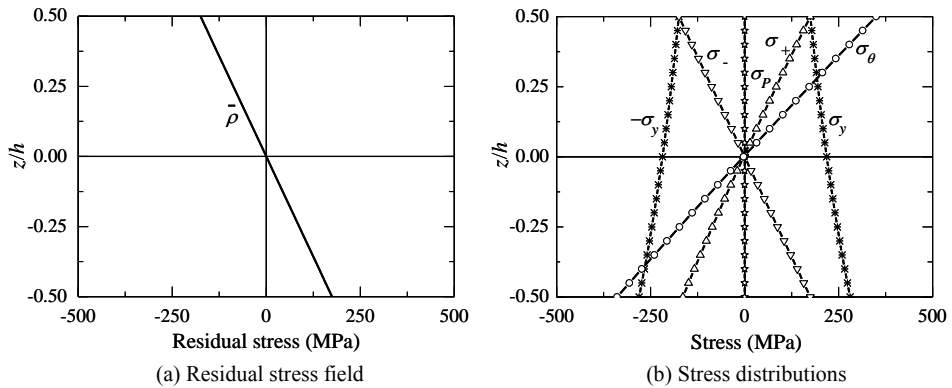


Figure 14: Stress distributions in Ti/Si₃N₄ FG plate corresponding to point E₂.

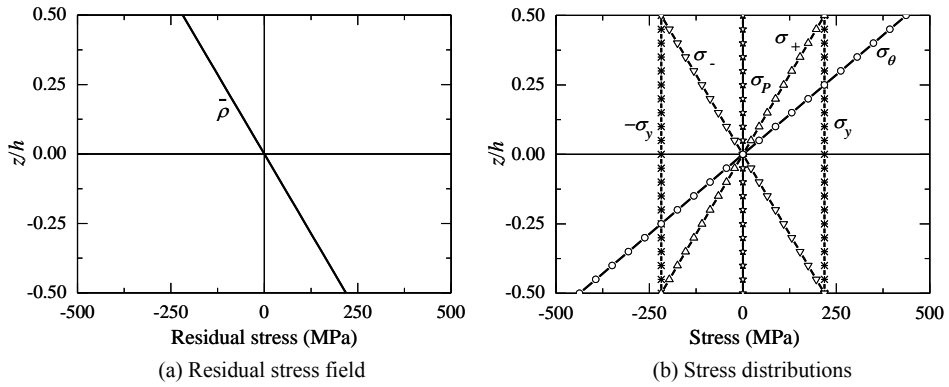


Figure 15: Stress distributions in Ti/Si₃N₄ effective homogenous plate corresponding to point E₃.

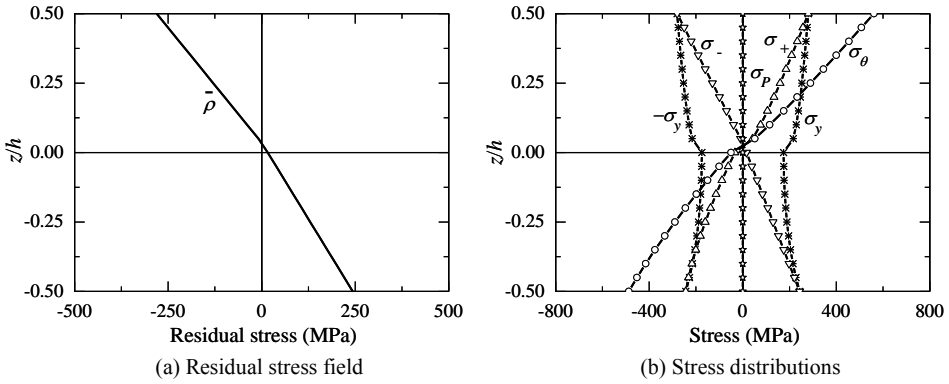


Figure 16: Stress distributions in Ti/Si₃N₄ FG plate corresponding to point E₄.

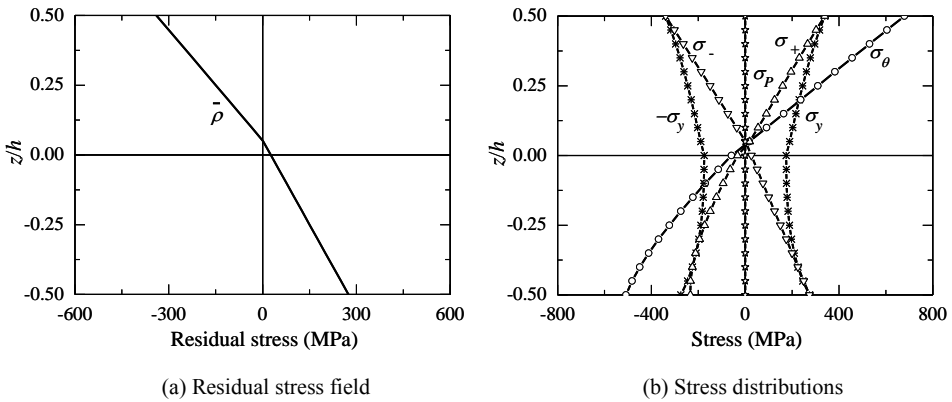


Figure 17: Stress distributions in Ti/Si₃N₄ FG plate corresponding to point E₅.

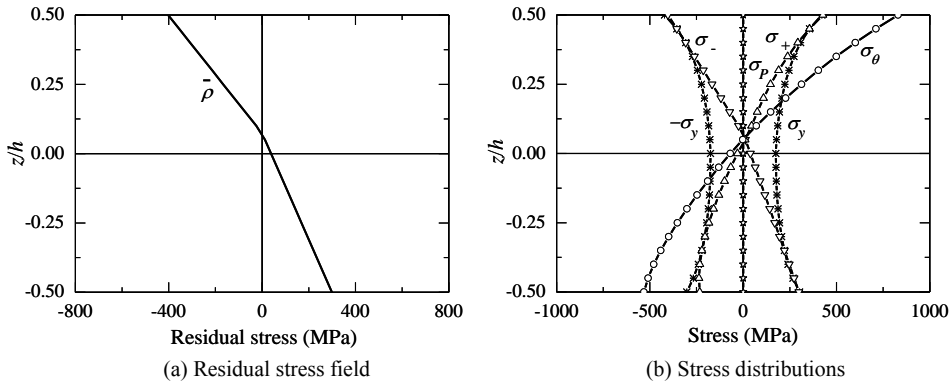


Figure 18: Stress distributions in Ti/Si₃N₄ FG plate corresponding to point E₆.

12. As shown in Figure 12, the plate of which the reinforcement phase volume fraction function is optimized can be endured larger $\Delta\bar{\theta}_{\max}$, i.e., $\Delta\bar{\theta}_{\max}$ of whichever Opt_0.3, Opt_0.4 and Opt_0.5 is larger than that of Homo_0.15.

The stress distributions corresponding to point E₄ on Opt_0.3, point E₅ on Opt_0.4 and point E₆ on Opt_0.5 have been respectively shown in Figures 16-18. In these figures the phenomena are similar with those in Figures 9-11, although the constituents of the FG plates are different.

5 Conclusion and discussion

The optimization of the volume fraction distribution function of reinforcement particles in FG Bree plates was performed with the GA approach. The objective of optimization was to gain the maximum of the $\Delta\bar{\theta}$ applied to the plates under the constraint that the average volume fraction of the reinforcement particles keeps constant. An optimal model was proposed and two numerical examples were presented, from which the following conclusion may be drawn:

1. An approach was developed for the optimization of the distribution of the reinforcement particles in the plate for the purpose to enhance the shakedown capability of the plate. The distribution of the material properties in the thickness of the plate was characterized with a piecewise exponential distribution, and the effective mechanical property of the material of the plate was evaluated with a double-inclusion mean field scheme, and the distribution of the volume fraction of the reinforcement particles was optimized with the Genetic Algorithm. The validity of the approach was demonstrated by the two numerical examples.

2. The shakedown capability of a FG plate is determined by both the applied thermal-mechanical loading and the thermal-mechanical properties of the plate. For a FG plate, the latter can be designed by properly distributing the volume fraction of the reinforcement particles, which provides the possibility to achieve desired or optimal thermal-mechanical properties of the plate to substantially enhance the shakedown capability of the plate. It was found in this paper that the distribution of the particle volume fraction affects markedly the shakedown capability of the FG plate, and a proper distribution of the particle volume fraction can substantially enhance the shakedown capability of the plate.
3. The concept of the piecewise distribution of the material properties is in accordance with that of the piecewise approach used in the shakedown analysis; therefore, it is of particular advantage for the optimization of the shakedown capability of the FG plate, because it may bring great convenience to the optimization without introducing additional difficulties.

Acknowledgement: The authors gratefully acknowledge the financial support to this work from NSFC under Grant Numbers 11272364 and 11332013.

References

- Andrew, J. G.; Senthil, S. V.** (2010): Transient multiscale thermoelastic analysis of functionally graded materials. *Compos. Struct.*, vol. 92, pp. 1372-1390.
- Aghababaei, R.; Reddy, J. N.** (2009): Nonlocal third-order shear deformation plate theory with application to bending and vibration of plates. *J. Sound Vib.*, vol. 326, pp. 277-289.
- Altenbach, H.; Eremeyev, V. A.** (2009): Eigen-vibrations of Plates made of Functionally Graded Material. *CMC: Computers, Materials, & Continua*, vol. 9, pp. 153-178.
- Bree, J.** (1967): Elastic plastic behavior of thin tubes subjected to internal pressure and intermittent high heat fluxes with application to fast nuclear reactor fuel elements. *J. Strain Anal.*, vol. 2, pp. 226-238.
- Cavalcanti, P. R; Carvalho, P. C. P; Martha, L. F.** (1997): Non-manifold modeling: an approach based on spatial subdivision. *Computer-Aided Design*, vol. 29, pp. 209-220.
- Chen, B.; Tong, L.** (2005): Thermo-mechanically coupled sensitivity analysis and design optimization of functionally graded materials. *Comput. Methods Appl. Mech. Eng.*, vol. 194, pp. 1891-1911.

- Chen, M.; Tucker, J. V.** (2000): Constructive volume geometry. *Comput. Graph. Forum*, vol. 19, pp. 281-293.
- Cheng, Z. Q.; Batra, R. C.** (2000): Three-dimensional thermoelastic deformations of a functionally graded elliptic plate. *Composites Part B*, vol. 31, pp. 97-106.
- Cho, J. R.; Choi, J. H.** (2004): A yield-criteria tailoring of the volume fraction in metal-ceramic functionally graded material. *Euro. J. Mech./A Solids*, vol. 23, pp. 271-281.
- Cho, J. R.; Ha, D. Y.** (2002): Volume fraction optimization for minimizing thermal stress in Ni-Al₂O₃ functionally graded materials. *Mater. Sci. Eng. A*, vol. 334, pp. 147-155.
- Cho, J. R.; Shin, S. W.** (2004): Material composition optimization for heat-resisting FGMs by artificial neural network. *Composites Part A: Applied Science and Manufacturing*, vol. 35, pp. 585-594.
- Dong, L.; Atluri, S. N.** (2012a): T-Trefftz voronoi cell finite elements with elastic/rigid inclusions or voids for micromechanical analysis of composite and porous materials. *CMES: Computers, Materials, & Continua*, vol. 83, pp. 183-219.
- Dong, L.; Atluri, S. N.** (2012b): Development of 3D Trefftz voronoi cells with ellipsoidal voids &/or elastic/rigid inclusions for micromechanical modeling of heterogeneous materials. *CMC: Computers Materials and Continua*, vol. 30, pp. 39-81.
- Dong, L.; Atluri, S. N.** (2013): SGBEM voronoi cells (SVCs), with embedded arbitrary-shaped inclusions, voids, and/or cracks, for micromechanical modeling of heterogeneous materials. *CMC: Computers, Materials & Continua*, vol. 33, pp. 111-154.
- Elishakoff, I.; Gentilini, C.** (2005): Three-dimensional flexure of rectangular plates made of functionally graded materials. *J. Appl. Mech.*, vol. 72, pp. 788-791.
- Feldoman, E.; Aboudi, J.** (1997): Buckling analysis of functionally graded plates subjected to uniaxial loading. *Compos. Struct.*, vol. 38, pp. 29-36.
- Guo, L. C.; Noda, N.** (2007): Modeling method for a crack problem of functionally graded materials with arbitrary properties piecewise exponential model. *Int. J. Solids Struct.*, vol. 44, pp. 6768-6790.
- Guo, L.; Wu, L.; Sun, Y.; Ma, L.** (2005): The transient fracture behavior for a functionally graded layered structure subjected to an in-plane impact load. *Acta Mech. Sinica*, vol. 21, pp. 257-266.
- Gilhooley, D. F.; Batra, R. C.; Xiao, J. R.; Mccarthy, M. A.; Gillespie, J. W.** (2007): Analysis of thick functionally graded plates by using higher-order shear and normal deformable plate theory and MLPG method with radial basis functions.

Compos. Struct., vol. 80, pp. 39-552.

Huang, J.; Fadel, G. M; Blouin, V. Y; Grujicic, M. (2002): Bi-objective optimization design of functionally gradient materials. *Materials and Design*, vol. 23, pp. 657-666.

Ju, J. W.; Chen, T. M. (1994): Micromechanics and effective moduli of elastic composites containing randomly dispersed ellipsoidal inhomogeneities. *Acta Mech.*, vol. 103, pp. 103- 121.

Khalil, S.; Nam, J.; Darling, A.; Sun, W. (2004): Multi-nozzle biopolymer deposition for freeform fabrication of tissue construct. In: *Proc. 15th solid freeform fabrication symposium*, pp.826-837.

Kou, X. Y.; Parks, G. T.; Tan, S. T. (2012): Optimal design of functionally graded materials using a procedural model and particle swarm optimization. *Computer-Aided Design*, vol. 44, pp. 300-310.

Kou, X. Y. (2006): Computer-aided design of heterogeneous objects. *Ph.D. thesis*. University of Hong Kong.

Kou, X. Y.; Tan, S. T.; Sze, W. S. (2006): Modeling complex heterogeneous objects with nonmanifold heterogeneous cells. *Computer-Aided Design*, vol. 38, pp. 457-474.

Kou, X. Y; Tan, S. T. (2009): Robust and efficient algorithms for rapid prototyping of heterogeneous objects. *Rapid Prototyping J.*, vol. 15, pp. 5-18.

König, J. A. (1987): Shakedown of elastic-plastic Structures. *PWN-Polish Scientific Publishers*.

Lee, Y. D.; Erdogan, F. (1994): Residual/thermal stress in FGM and laminated thermal barrier coating. *Int. J. Fracture*, vol. 69, pp. 145-165.

Na, K. S.; Kim, J. H. (2006): Three-dimensional thermomechanical buckling analysis for functionally graded composite plates. *Compos. Struct.*, vol. 73, pp. 413-422.

Noda, N.; Tsuji, T. (1990): Steady thermal stresses in a plate of functionally gradient material. *Proc. 1st Int. Symp. Functionally Gradient Materials*, pp. 339–344.

Markworth, A. J.; Saunders, J. H. (1995): A model of structure optimization for functionally graded materials. *Mater. Lett.*, vol. 22, pp. 103–107.

Ootao, Y.; Kawamura, R.; Tanigawa, Y.; Imamura, R. (1999): Optimization of material composition of nonhomogeneous hollow sphere for thermal stress relaxation making use of neural network. *Comput. Methods Appl. Mech. Eng.*, vol. 180, pp. 185-201.

Parashkevova, L.; Ivanova, J.; Bontcheva, N. (2004): Optimal design of func-

tionally graded plates with thermo-elastic-plastic behavior. *Comptes Rendus Mecanique*, vol. 332, pp. 493-498.

Peng, X.; Fan, J.; Zeng, X. (1996): Analysis for plastic buckling of thin-walled cylinders via non-classical constitutive theory of plasticity. *In. J. Solids and Struct.*, vol. 33, pp. 4495-4509.

Peng, X.; Hu, N.; Zheng, H.; Fang, C. (2009a): Analysis of shakedown of FG Bree plate subjected to coupled thermal-mechanical loadings. *Acta Mech. Solida Sinica*, vol. 22, pp. 95-108.

Peng, X.; Ponter, A.R.S. (1993): Extremal properties of Endochronic plasticity, Part II: Extremal path of the Endochronic constitutive equation with a yield surface and application. *Int. J. Plasticity*, vol. 9, pp. 567-581.

Peng, X.; Zheng, H.; Hu, N.; Fang, C. (2009b): Static and kinematic shakedown analysis of FG plate subjected to constant mechanical load and cyclically varying temperature change. *Composite Structures*, vol. 91, pp. 212-221.

Praveen, G. N.; Reddy, J. N. (1998): Nonlinear transient thermoelastic analysis of functionally graded ceramic-metal plates. *Int. J. Solids and Struct.*, vol. 35, pp. 4457-4476.

Qiu, J.; Tani, J.; Warkentin, D. J. (1999): Stress analysis of RAINBOW actuators and relief of stress by gradation of material composition. *Japan. Soc. Appl. Electromagn. Mech.*, vol. 7, pp. 185192

Reddy, J. N. (2011): Microstructure-dependent couple stress theories of functionally graded beams. *J. Mech. Phys. Solids*, vol. 59, pp. 2382-2399.

Shen, Y. (1998): Thermal expansion of metal–ceramic composites: a three-dimensional analysis. *Mater. Sci. Eng. A*, vol. 252, pp. 269-275.

Suresh, S.; Mortensen, A. (1998): Fundamentals of functionally graded materials: processing and thermomechanical behaviour of graded metals and metal-ceramic composites. *IOM Communications Ltd, London*.

Suresh, S.; Mortensen, A. (1998): Fundamentals of functionally graded materials. *London, UK: Institute of Materials*.

Tani, J.; Qiu, J.; Morit, A. T. (2001): Functionally gradient piezoelectric actuators *Trans. Mater. Res. Soc. Japan*, vol. 26, pp. 283286

Vel, S. S.; Batra, R. C. (2002): Exact solution for thermoelastic deformations of functionally graded thick rectangular plates. *AIAA J.*, vol. 40, pp. 1421-1433.

Vel, S.S.; Batra, R.C. (2003): Three-dimensional analysis of transient thermal stresses in functionally graded plates. *Int. J. Solids.Struct.*, vol. 40, pp. 7181-7196.

Wadley, H. N. G.; Fleck, N. A.; Evans, A. G. (2003): Fabrication and structural

performance of periodic cellular metal sandwich structures. *Compos. Sci. Technol.*, vol. 63, pp. 2331- 2343.

Wang, B. L.; Han, J. C.; Du, S. Y. (2000): Crack problems for functionally graded materials under transient thermal loading. *J. Thermal Stresses*, vol. 23, pp. 143-168.

Watari, F.; Yokoyama, A.; Omori, M.; Hirai, T.; Kondo, H.; Uo, M.; Kawasaki, T. (2004): Biocompatibility of materials and development to functionally graded implant for biomedical application. *Compos. Sci. Technol.*, vol. 64, pp. 893-908.

Williams, C. B.; Mistree, F.; Rosen, D. W. (2005): Investigation of additive manufacturing processes for the manufacture of parts with designed mesostructure. *In: Proc. ASME 2005 design engineering technical conferences*, pp. 353-364.

Wu, C. P.; Huang, S. E. (2009): Three-Dimensional Solutions of Functionally Graded Piezo-Thermo-Elastic Shells and Plates Using a Modified Pagano Method. *CMC: Computers, Materials, & Continua*, vol. 12, pp. 251-282.

Zheng, H.; Peng, X.; Hu, N. (2012): Analysis for Shakedown of Functionally Graded Plate Subjected to Thermal-Mechanical Loading with Piecewise-Exponential Distribution of Material Properties. *CMES: Comp. Model. Eng. Sci.*, vol. 86, pp. 505-531.

Zhong, Z.; Shang, E. T. (2003): Three-dimensional exact analysis of simply supported functionally gradient piezoelectric plates. *Int. J. Solids Struct.*, vol. 40, pp. 5335-5352.